

Efficient reinforcement learning with partially observable for fluid flow controlA. Kubo¹ and M. Shimizu^{1, a)}*Graduated School of Engineering Science, Osaka University, Toyonaka,
560-0043 Japan*

(Dated: 25 November 2021)

Despite the low dimensionalities of dissipative viscous fluids, reinforcement learning (RL) requires many observables in fluid control problems. This is because the observables are assumed to follow a policy-independent Markov decision process in the RL framework. By including policy parameters as arguments of a value function, we construct a consistent algorithm with partially observable condition. Using typical examples of active flow control, we show that our algorithm is more stable and efficient than the existing RL algorithms, even under a small number of observables.

arXiv:2012.04138v2 [physics.flu-dyn] 29 Apr 2021

^{a)}Electronic mail: shimizu@me.es.osaka-u.ac.jp

I. INTRODUCTION

Data-driven modeling based on machine learning is currently more practical than conventional modeling based on theories in various applications including fluid engineering. Machine learning is used to model, control, and optimize flows from the vast amount of data obtained from experiments and simulations. For a detailed review of machine-learning applications in fluid mechanics, refer to Brunton et al. (2020)¹.

Reinforcement learning (RL)² is one of machine learning techniques. Its algorithm finds the optimal control method that maximizes the total rewards in a given system. The learning algorithms adopt a trial-and-error approach to determine the optimal control from the time-series of states, actions, and rewards. Recently, deep reinforcement learning (DRL)³, the combination of deep learning and RL, has achieved unprecedented performance in artificial intelligence. The first successful examples of applications include Go, Shogi, and other video games. These systems significantly outperform the best human players⁴. DRL has also been successfully applied to industrial applications such as autonomous driving⁵ and controlling of robots⁶.

Previous studies have also investigated the applicability of RL in active control, optimal design, and numerical modeling within fluid mechanics. Value-based RL with Q-learning or SARSA has been applied in school movement optimization⁷⁻⁹, reduction of drag around cylinders¹⁰, and optimal glider control^{11,12}. Verma et al. (2018) combined deep long short-term memory with RL to investigate the mechanism of fish school formation¹³. In recent years, DRL based on a kind of actor-critic algorithm has been applied to flow control problems. Many researchers have applied DRL to optimal flow control, including fish adaption behaviors¹⁴, drag reduction around a cylinder (blowing/suction¹⁵⁻¹⁸, rotary oscillations¹⁹, and assistant rotating cylinders²⁰), optimal control of Rayleigh–Bénard convection²¹, conjugate heat transfer²², and shape optimization problems²³. Moreover, DRL has been applied to the construction of efficient numerical models, optimal simulation hyperparameters²⁴, and optimal large eddy simulation²⁵. See recent reviews^{26,27} for more details of DRL within fluid flow control.

Generally, RL algorithms assume the time evolution as a Markov decision process that does not depend on the means of control (policy). However, this assumption usually fails when learning is performed in a partially observable condition. Although fluid systems have infinite degrees of freedom, the number of observations is limited in practical control. In a dissipative system, such as a viscous fluid, the system's final state (attractor) requires only a finite number of observables to

determine the state.²⁸ Because these finite observables can describe the time evolution, their time series can be regarded as a Markov process. However, this process depends on policy: the way of time evolution among these observables depends on the way of control. Therefore, in principle we cannot apply existing RL directly to a problem of fluid control with partially observable conditions even if the number of observables is enough to capture the dynamics. In this paper, we describe a framework that resolves the above frustrating contradiction and optimally controls fluid with a small number of observables, and adapt it to a few typical active-control problems as benchmark examples..

II. ALGORITHM

A. Deterministic Actor-Critic Algorithm

Before introducing our new algorithm, we describe the outline of the existing RL algorithm only for the on-policy deterministic actor-critic method²⁹ to simplify the analysis. Most of previous studies using DRL for fluid control are based on the actor-critic method. Here, we assume that our system evolves deterministically, and control is determined as a function of the state. These assumptions may be sufficient for fluid control. If exploration is to be considered, the algorithm can be changed to an off-policy type, according to the approach described by Silver et al. (2014)²⁹.

We consider a discrete dynamical system given by the deterministic map F (deterministic Markov decision process):

$$\mathbf{s}_{t+1} = F(\mathbf{s}_t, \mathbf{a}_t), \quad (1)$$

where, \mathbf{s}_t is the state of the system at time t , and \mathbf{a}_t is the control to the system (action). In the deterministic policy framework, the action is a function of a state, $\mathbf{a}_t = \boldsymbol{\mu}(\mathbf{s}_t)$, where $\boldsymbol{\mu}$ determines the means of control and is called the policy. Generally, a policy is approximated by a parametric function such as $\boldsymbol{\mu}(\mathbf{s}) \simeq \tilde{\boldsymbol{\mu}}(\mathbf{s}; \boldsymbol{\theta})$. Here, the parameters $\boldsymbol{\theta}$ are called design variables and are optimized to maximize the objective function defined below. Hereafter, $\tilde{\cdot}$ represents a parametric function. Let the reward be $r_t = R(\mathbf{s}_t, \mathbf{a}_t)$. Then, we define the value function V and the objective

function J as follows:

$$V(\mathbf{s}; \boldsymbol{\theta}) = \sum_{t=0}^{\infty} \gamma^t r_t(\mathbf{s}_t, \mathbf{a}_t) |_{\mathbf{s}_0=\mathbf{s}}, \quad (2)$$

$$J(\boldsymbol{\theta}) = \lim_{T \rightarrow \infty} \frac{1}{T} \sum_{t=0}^{T-1} V(\mathbf{s}_t; \boldsymbol{\theta}) = \int_{\mathbf{s}} \rho(\mathbf{s}; \boldsymbol{\theta}) V(\mathbf{s}; \boldsymbol{\theta}) d\mathbf{s}, \quad (3)$$

where, γ is a discount rate and satisfies $0 \leq \gamma < 1$, and ρ represents the probability density in the state space. V means the weighted sum of reward r_t , and J is its average. In the limit of $\gamma \rightarrow 0$, J simply represents the average reward. Optimal control determines the optimal design parameters $\boldsymbol{\theta}^*$ that maximize the objective function as

$$\boldsymbol{\theta}^* = \arg \max_{\boldsymbol{\theta}} J(\boldsymbol{\theta}), \quad (4)$$

$$\tilde{\boldsymbol{\mu}}^*(\mathbf{s}) = \tilde{\boldsymbol{\mu}}(\mathbf{s}; \boldsymbol{\theta}^*). \quad (5)$$

When the time series of the state is a stationary process such as an attractor in a dissipative system, $\boldsymbol{\theta}^*$ is independent of γ . This is because γ changes J only by a constant multiple. In the actor-critic method, the objective function J is optimized via the action-value function Q as

$$Q(\mathbf{s}, \mathbf{a}; \boldsymbol{\theta}) = \sum_{t=0}^{\infty} \gamma^t r_t(\mathbf{s}_t, \mathbf{a}_t) |_{\mathbf{s}_0=\mathbf{s}, \mathbf{a}_0=\mathbf{a}}. \quad (6)$$

As for the policy, the action-value function is approximated by the parametric function of $\boldsymbol{\omega}$ such that $Q(\mathbf{s}, \mathbf{a}; \boldsymbol{\theta}) \simeq \tilde{Q}(\mathbf{s}, \mathbf{a}; \boldsymbol{\theta}, \boldsymbol{\omega})$. At the end of every episode, the critic updates \tilde{Q} , following the SARSA method, as

$$\delta_t = r_{t+1} + \gamma \tilde{Q}(\mathbf{s}_{t+1}, \mathbf{a}_{t+1}; \boldsymbol{\theta}_n, \boldsymbol{\omega}_n) - \tilde{Q}(\mathbf{s}_t, \mathbf{a}_t; \boldsymbol{\theta}_n, \boldsymbol{\omega}_n), \quad (7)$$

$$\boldsymbol{\omega}_{n+1} = \boldsymbol{\omega}_n + \alpha_{\omega} \sum_{t \in T_n} \delta_t \nabla_{\omega} \tilde{Q}(\mathbf{s}_t, \mathbf{a}_t; \boldsymbol{\theta}_n, \boldsymbol{\omega}_n), \quad (8)$$

where, the subscript n represents the episode number, $T_n = \{t_{n1}, t_{n2}, \dots, t_{nN}\}$ is the set of N samples at n -th episode, and α_{ω} is the learning rate for $\boldsymbol{\omega}$. On the other hand, the actor follows the deterministic policy gradient theorem²⁹ given by

$$\nabla_{\boldsymbol{\theta}} J(\boldsymbol{\theta}) = \int_{\mathbf{s}} \rho(\mathbf{s}; \boldsymbol{\theta}) \nabla_{\boldsymbol{\theta}} \tilde{\boldsymbol{\mu}}(\mathbf{s}; \boldsymbol{\theta}) \nabla_{\mathbf{a}} \tilde{Q}(\mathbf{s}, \mathbf{a}; \boldsymbol{\theta}) |_{\mathbf{a}=\tilde{\boldsymbol{\mu}}(\mathbf{s}; \boldsymbol{\theta})} d\mathbf{s}, \quad (9)$$

and updates the design variables by the stochastic gradient as

$$\boldsymbol{\theta}_{n+1} = \boldsymbol{\theta}_n + \alpha_{\theta} \sum_{t \in T_n} \nabla_{\boldsymbol{\theta}} \tilde{\boldsymbol{\mu}}(\mathbf{s}_t; \boldsymbol{\theta}_n) \nabla_{\mathbf{a}} \tilde{Q}(\mathbf{s}_t, \mathbf{a}_t; \boldsymbol{\theta}_n), \quad (10)$$

where, α_θ is the learning rate for the design variables. The summation of the second term gives an unbiased estimate of the policy gradient (9).

From the set of time-series data $(\mathbf{s}_t, \mathbf{a}_t, r_t)$, the actor-critic method determines the optimal policy $\tilde{\mu}^*$ by repeatedly updating the action value function \tilde{Q} and the policy $\tilde{\mu}$ according to the equations (8) and (10), respectively. Note that in the derivation of the stochastic gradient (10), the dynamics of the system F and the reward R should not depend directly on the policy; that is, $\frac{\partial F_i}{\partial \theta_i} = 0$ and $\frac{\partial R}{\partial \theta_i} = 0$. For details of the derivation, see Silver et al. (2014)²⁹ and Sutton et al. (1999)³⁰.

B. Algorithm for Fluid Systems

In a dissipative system, such as a viscous fluid, the solution trajectory of the final state of the system is often in a much lower dimensional space (attractor) than that of the system²⁸. Assuming that the capacity dimension of the attractor is D_e , the state can be specified in most cases with $2[D_e] + 1$ observables²⁸. ($[\cdot]$ represents the Gauss sign.) For example, we can determine the state of a microorganism that swims in water with periodic motion using only three variables. Let \mathbf{o} be N_o observables sufficient to uniquely determine each moment on the attractor. The transition among the partial observables \mathbf{o} is given by the map $\mathbf{o}_{n+1} = \mathbf{F}(\mathbf{o}_t, \tilde{\mu}(\mathbf{o}_t); \boldsymbol{\theta})$, and it depends on the policy, $\boldsymbol{\theta}$. The deterministic Markov process defined by the equation (1) is independent of the policy only when all variables \mathbf{s} are observed; the state \mathbf{s} evolves according to the Navier–Stokes equations with the external control, which depends only on \mathbf{s} . As mentioned in the previous subsection, the policy ($\boldsymbol{\theta}$) independence of the evolution of a system is a necessary condition of the policy gradient theorem.^{29,30} Thus, even if the attractor is low dimensional, many observations are required to update a policy appropriately when using typical RL algorithms for fluid control problems. In the following discussion, we construct the consistent algorithm with partially observable.

The value function can be determined with the minimum number of arguments by specifying \mathbf{o} and $\boldsymbol{\theta}$. Therefore, there exists \hat{V} such that

$$V(\mathbf{s}; \boldsymbol{\theta}) = \hat{V}(\mathbf{o}, \boldsymbol{\theta}). \quad (11)$$

We approximate \hat{V} as a parametric function for \mathbf{w} as

$$\hat{V}(\mathbf{o}, \boldsymbol{\theta}) \simeq \tilde{V}(\mathbf{o}, \boldsymbol{\theta}; \mathbf{w}) = \mathbf{w}^T \boldsymbol{\phi}(\mathbf{o}, \boldsymbol{\theta}), \quad (12)$$

where, ϕ_i are nonlinear basis functions of \mathbf{o} and $\boldsymbol{\theta}$, which are constructed from the time-series data. The construction in this paper will be shown below. We assume that the policy is a linear function of the observable \mathbf{o} :

$$\tilde{\boldsymbol{\mu}}(\mathbf{o}; \boldsymbol{\theta}) = \boldsymbol{\Theta} \mathbf{o}, \quad (13)$$

where $\boldsymbol{\Theta}$ is matrix representation for $\boldsymbol{\theta}$; $\Theta_{ij} = \theta_{(i-1)N_o+j}$. Arbitrary control becomes possible by increasing the number of observables. Otherwise, the use of nonlinear basis functions enables complex control.

In our proposed algorithm, the critic and the actor work as follows. The critic updates \tilde{V} every N_e steps of a numerical simulation. The unit of this update is called the *episode*. The weight \mathbf{w}_n of \tilde{V} at the end of the n -th episode is calculated as follows:

$$\delta_t = \sum_{k=0}^{N_s-1} \gamma^k r_{t+k} + \gamma^{N_s} \tilde{V}(\mathbf{o}_{t+N_s}, \boldsymbol{\theta}_{t+N_s}) - \tilde{V}(\mathbf{o}_t, \boldsymbol{\theta}_t), \quad (14)$$

$$\mathbf{w}_n = \arg \min_w \sum_{t \in T_n} \delta_t^2, \quad (15)$$

where, δ_t represents the N_s step TD error. $T_n = \{(n-M)N_e, (n-M)N_e + 1, \dots, nN_e - 1\}$ is the set of steps in the last M episodes. The basis functions ϕ are constructed from the time series $\{(\mathbf{o}_t, \boldsymbol{\theta}_t) | t \in T_n\}$. We use the RBF sampler³¹ of the package scikit-learn³² for the basis functions. Then, the actor calculates the stochastic gradient \mathbf{g}_n at the n -th episode by the linear regression algorithm:

$$\mathbf{g}_n, b_n = \arg \min_{\mathbf{g}, b} \sum_{t \in T_n} (\mathbf{g}^T \boldsymbol{\theta}_t + b - \tilde{V}(\mathbf{o}_t, \boldsymbol{\theta}_t))^2. \quad (16)$$

In both minimization problems, given by equations (15) and (16), the singular value decomposition is used to avoid singularities of linear equations. Using the gradient, \mathbf{g}_n , the policy is updated at each time step in episode n as follows:

$$\boldsymbol{\theta}_{t+1} = \boldsymbol{\theta}_t + \alpha \mathbf{g}_n, \quad (17)$$

where, α is the learning rate. In the limit $\alpha \rightarrow 0$, the orbit \mathbf{o}_t changes in a quasi-static manner, and \tilde{V} is defined on the attractor.

III. BENCHMARK RESULTS

A. Drag reduction through blowing and suction

We apply the proposed algorithm to the active flow control problem³³ to validate its effectiveness. The goal of this problem is to minimize the magnitude of the drag acting on a cylinder by controlling the mass flow rate of two synthetic jets symmetrically located on the top and bottom of a cylinder immersed in a two-dimensional incompressible fluid.

The flow configuration and optimization problem have been adopted from Rabault et al. (2019)³³. The difference from previous settings is that (i) the policy function is a linear function (13) rather than a nonlinear function constructed with a neural network, and (ii) the policy parameters are updated with the proposed algorithm in §II B instead of proximal policy optimization (PPO)³⁴.

The flow in this system follows the governing non-dimensional equations given by

$$\nabla \cdot \mathbf{u} = 0 \quad \text{in } \Omega, \quad (18)$$

$$\frac{\partial \mathbf{u}}{\partial t} + (\mathbf{u} \cdot \nabla) \mathbf{u} = -\nabla p + \frac{1}{\text{Re}} \Delta \mathbf{u} \quad \text{in } \Omega, \quad (19)$$

$$\mathbf{u} = \frac{6}{4.1^2} \left(\frac{4.1}{2} - y \right) \left(\frac{4.1}{2} + y \right) \mathbf{e}_x \quad \text{on } \Gamma_{\text{in}}, \quad (20)$$

$$-pn + \frac{1}{\text{Re}} \nabla u n = 0 \quad \text{on } \Gamma_{\text{out}}, \quad (21)$$

$$\mathbf{u} = 0 \quad \text{on } \Gamma_{\text{wall}}, \quad (22)$$

$$\mathbf{u} = Q_1 \frac{\pi}{10} \cos \left(\frac{\pi}{10} (\varphi - 90) \right) \mathbf{e}_r \quad \text{on } \Gamma_1, \quad (23)$$

$$\mathbf{u} = Q_2 \frac{\pi}{10} \cos \left(\frac{\pi}{10} (\varphi - 270) \right) \mathbf{e}_r \quad \text{on } \Gamma_2, \quad (24)$$

where Ω is a whole computational domain; Γ_{in} is an inflow boundary; Γ_{out} is an outflow boundary; Γ_{wall} is a no-slip boundary—that is, top and bottom walls and the solid walls of the cylinder except for the jet parts $\Gamma_i, i = 1, 2$; and \mathbf{e}_x and \mathbf{e}_r denote unit vectors in the streamwise (x -) and radius direction, respectively. It should be noted that the two jets (jet 1 and jet 2) are implemented on the cylinder as angles $\varphi = 90^\circ$ and 270° , respectively, and the total mass flow rate injected by them is set to null—i.e., $Q_1 + Q_2 = 0$ and $|Q_1| \leq 0.1$, where φ is an angle from the streamwise (x -) direction. The Reynolds number Re based on the bulk mean streamwise velocity and cylinder diameter is set to 100.

Pressures on the probes located in the vicinity of the cylinder and near the wake are observed.

In the previous study, learning was performed in three cases of 5, 11, and 151 pressure probes, but in this study, only two cases of 5 and 11 are conducted.

The reward function is defined by

$$r_t = -\langle C_D \rangle_T - 0.2|\langle C_L \rangle_T|, \quad (25)$$

where $\langle \cdot \rangle_T$ denotes the sliding average back in time over a duration corresponding to one vortex shedding cycle. C_D and C_L are the drag and lift coefficients on the cylinder (Γ_{cylinder}) given by

$$C_D = \int_{\Gamma_{\text{cylinder}}} 2(\boldsymbol{\sigma}\mathbf{n}) \cdot \mathbf{e}_x d\Gamma, \quad (26)$$

$$C_L = \int_{\Gamma_{\text{cylinder}}} 2(\boldsymbol{\sigma}\mathbf{n}) \cdot \mathbf{e}_y d\Gamma, \quad (27)$$

respectively, where, $\boldsymbol{\sigma}$ is the Cauchy stress tensor and \mathbf{e}_y is a unit vector in the wall-normal (y-) direction.

The trick to help the agent learning is implemented³³: the mass flow rate by two jets is obtained as $Q_{i,t+1} = Q_{i,t} + 0.1(0.1 \tanh(a_{i,t}) - Q_{i,t})$, where $Q_{i,t}$ and $a_{i,t}$ are the mass flow rate and the action, respectively, at time t of jet i .

We use their open-source code and replace only the RL part of that code with our proposed algorithm above. The parameters of RL are as follows: $N_s = 200, N_e = 4000, M = 20$, and $\alpha = 0.0002(1 - \frac{n}{500+M})$. 4000 steps correspond to 20 dimensionless times (the numerical time step is set to 5×10^{-3}) and approximately six vortex shedding periods in the case without blowing/suction control. In the first M episodes ($1 \leq n \leq M$), the policy gradient \mathbf{g}_n is given randomly.

Figure 1 shows the learning history, where N_o denotes the number of observables (pressure probes in this problem). From this figure, it can be seen that the drag coefficient C_D decreases more stably when learning using the proposed algorithm compared to that in the previous studies with stochastic policies. This is mainly because the optimization process in the proposed algorithm is deterministic, and the trajectory remains close to an attractor for each policy parameter $\boldsymbol{\theta}$. The time variation of C_D obtained according to the optimal policy for each case is shown in Fig.2. In the case of $N_o = 11$, we consider $\boldsymbol{\theta}$ at the 446th episode, which is approximately 10 episodes before the local minimum of the objective function, as the optimal policy. Immediately after this local minimum, the flow becomes unstable, and the stochastic gradient fails to increase the objective function. In the statistical stationary state, after a sufficiently long term from the initial condition, our linear policy with $N_o = 11$ has achieved slightly larger drag reduction compared to a previous study³³ adopting a large-scale neural network policy function with $N_o = 151$.

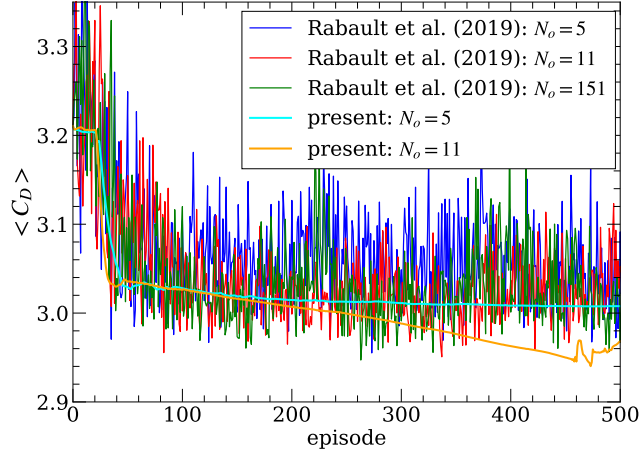


FIG. 1. Learning history of the blowing/suction problem. $\langle C_D \rangle$ is the time-averaged drag coefficient C_D within one episode.

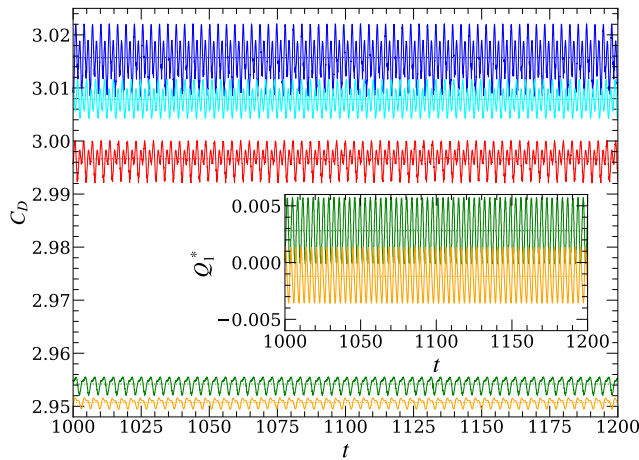


FIG. 2. Time variation of the drag coefficient C_D (lines). The dotted lines represent the time averaged value for each case. Each color represents the same case as in Fig. 1. The inset shows the time series of normalized mass flow rate Q_1^{*33} .

B. Optimization of propulsion direction

For the second demonstration, we consider a cylinder driven by a constant-magnitude external force \mathbf{F} in a 2D incompressible flow field (Fig. 3). The Reynolds number Re based on the external force is set to 100, and thus a vortex street is observed in the wake of the cylinder, leading to suppression of the cylinder movement. The cylinder is a rigid body whose mass density ρ_c is two times larger than that of the fluid ρ_f —i.e., $\rho_r = \rho_c/\rho_f = 2$ —and its rotational motion is ignored

for simplicity. The goal here is to maximize the time-averaged velocity $\langle V_x \rangle$ of the cylinder by controlling the direction β of the external force.

The flow \mathbf{u} and cylinder velocity $\mathbf{V}(= (V_x, V_y)^T)$ in this system follow the governing non-dimensional equations given by

$$\nabla \cdot \mathbf{u} = 0, \quad \text{in } \Omega_f, \quad (28)$$

$$\frac{\partial \mathbf{u}}{\partial t} + (\mathbf{u} \cdot \nabla) \mathbf{u} = -\nabla p + \frac{1}{\text{Re}} \Delta \mathbf{u} + \mathbf{f}_{\text{damp}}, \quad \text{in } \Omega_f, \quad (29)$$

$$\mathbf{u}(x, y) = \mathbf{u}(x + 50, y) = \mathbf{u}(x, y + 10) \quad \text{in } \Omega_f, \quad (30)$$

$$\rho_r \frac{d\mathbf{V}}{dt} = \int_{\partial\Omega_c} \boldsymbol{\sigma} n d\mathbf{x} + (\cos \beta, \sin \beta)^T, \quad (31)$$

where Ω_f is fluid domain. Periodic boundary conditions are imposed on the x - and y -directions, and their periods are taken as 50 and 10, respectively, but the flow is stopped by the damping term \mathbf{f}_{damp} in region 40 downstream from the cylinder to eliminate the inflowing vortex.

DNS is performed in a noninertial system with a fixed cylinder, and the immersed boundary method is employed for the object representation³⁵. The uniform staggered grids are employed with the number of grid points being 500×50 in the x - and y -directions and the numerical time step is 10^{-2} .

The observables are the y -component of velocity V_y of the cylinder, lift $L = C_L/2$ (see (27)) and time-delayed values of these two quantities: $\boldsymbol{o}_t = (V_{y,t}, L_t, V_{y,t-N_s}, L_{t-N_s}, V_{y,t-2N_s}, L_{t-2N_s}, \dots)^T$. The reward is defined as $r_t = V_{x,t}$. The parameters of RL are $N_s = 100, N_e = 5000, M = 20$, and $\alpha = 10^{-4 - \lfloor \frac{n}{500+M} \rfloor}$ ($\lfloor \cdot \rfloor$ represents the Gauss sign). 5000 steps correspond to approximately four vortex shedding periods in the case when external forces are applied from a constant angle $\beta = 0$.

Figure 4 shows the learning history in the cases of $N_o = 2, 4$ and 8. As the number of observables increases, the objective function increases rapidly. The performance with $N_o = 8$ is improved by approximately 1% compared to the case when external forces are applied from a constant angle. Fig. 5 represents difference in trajectories among these three cases. In this control problem, the flow becomes unstable when the cylinder velocity is relatively high. Thus, for successful and stable learning, we must adjust the learning rate α to be small around an optimal design variable.

C. Speed maximization of a swimming hinge

For the third demonstration, we consider a swimming hinge with infinitesimal thickness, driven by an external torque $T \leq T_{\text{max}}$ in a 2D incompressible flow field (Fig. 6). The torque acts only on

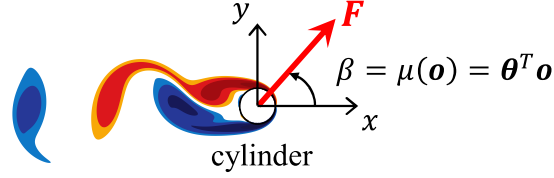


FIG. 3. Configuration of the cylinder forcing problem. Reinforcement learning optimizes the policy β , the direction of forcing, to maximize the average speed of the cylinder $\langle V_x \rangle$.

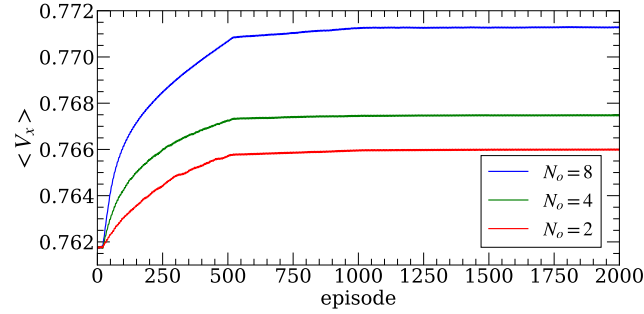


FIG. 4. Learning history of the cylinder forcing problem. $\langle V_x \rangle$ is the time-averaged V_x per episode.

the plate 1, and the plate 2 is allowed to move only in the x -direction.

The Reynolds number Re based on the maximum torque is set to 100, and thus, a vortex street is observed in the wake of the object, leading to suppression of the movement. The object is a rigid body whose mass density is 1.1 times larger than that of the fluid, that is $\rho_r = 1.1$. The goal here is to maximize the time-averaged velocity $-\langle x_h \rangle$ of the object by controlling the magnitude of the external torque $T = \tanh(\tilde{\mu}) + 0.1 \sin(2\pi t/5)$. The second term of this torque is introduced to escape stably from null state; the speed of the object driven only by this term is approximately 0.02, which is small enough compared with the speed under the following optimum control ~ 0.5 .

The velocity fields \mathbf{u} and the positions of the joint point x_h in this system follow the governing non-dimensional equations given by

$$\nabla \cdot \mathbf{u} = 0 \quad \text{in } \Omega_f, \quad (32)$$

$$\frac{\partial \mathbf{u}}{\partial t} + (\mathbf{u} \cdot \nabla) \mathbf{u} = -\nabla p + \frac{1}{Re} \Delta \mathbf{u} \quad \text{in } \Omega_f, \quad (33)$$

$$\mathbf{u} = (\dot{x}_h - d\dot{\beta} \sin \beta, 0)^T \quad \text{in } \Omega_1, \quad (34)$$

$$2\rho_r \ddot{x}_h - \frac{\rho_r}{2} (\ddot{\beta} \sin \beta + \dot{\beta}^2 \cos \beta) = G_x, \quad (35)$$

$$\frac{\rho_r}{3} \ddot{\beta} - \frac{\rho_r}{2} \ddot{x}_h \sin \beta = K + T, \quad (36)$$

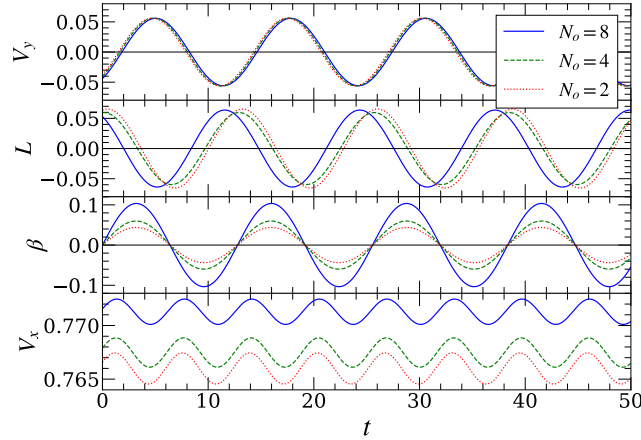


FIG. 5. Trajectories of the observables V_y, L , the action β , and the reward V_x under the optimal policies for different numbers of observables N_o .

where Ω_f and Ω_i are fluid and plate i , respectively. Dot notation represents derivative with respect to time. d is the one-dimensional coordinate on the flat plate 1 with the hinge as the origin, and β is the angle formed by the flat plate 1 from the x -direction. \mathbf{G} denotes the sum of the force acting on the hinge from the viscous stress, $\mathbf{G} = \int_{\partial\Omega_1 + \partial\Omega_2} \boldsymbol{\sigma} \mathbf{n} \, dx$ and K the sum of the torque acting on the rotational plate 1 from the viscous stress, $K = \int_{\partial\Omega_1} [\mathbf{x} \times (\boldsymbol{\sigma} \mathbf{n})]_z \, dx$.

DNS is performed in a non-inertial system in which the joint point is fixed at the origin, and the immersed boundary method is employed to solve fluid–structure interaction³⁵. The uniform staggered grids are employed with the number of grid points being 400×400 in the x - and y -directions and the numerical time step is 5×10^{-3} .

The observables are the angle and angular velocity of flat plate 1 and time delayed values of these two quantities: $\mathbf{o}_t = (\beta_t, \dot{\beta}_t, \beta_{t-N_s}, \dot{\beta}_{t-N_s}, \beta_{t-2N_s}, \dot{\beta}_{t-2N_s}, \dots)^T$. The reward is defined as $r_t = -\dot{x}_{h,t}$. The parameters of reinforcement learning are $N_s = 200, N_e = 4000, M = 10$, and $\alpha = \text{Max}(10^{-5 - \lfloor \frac{n}{500+M} \rfloor}, 10^{-7})$.

Figure 7 shows the learning history in the cases of $N_o = 2, 4$ and 8 . As in the example of the previous subsection, the objective function increases rapidly as the number of observables increases. However, the dependence on the number of observables on the optimal values is larger than the previous problem, and the objective function $-\langle \dot{x}_h \rangle$ doesn't improve at all for $N_o = 2$.

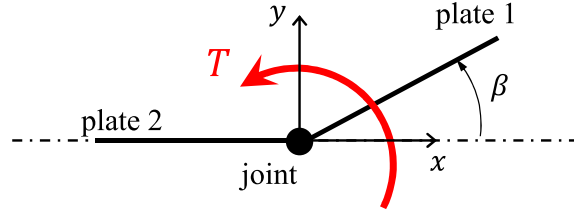


FIG. 6. Configuration of the swimming problem. The hinge is driven by the external torque T acting on the plate 1. Reinforcement learning optimizes T to maximize the average speed of the hinge $-\langle \dot{x}_h \rangle$.

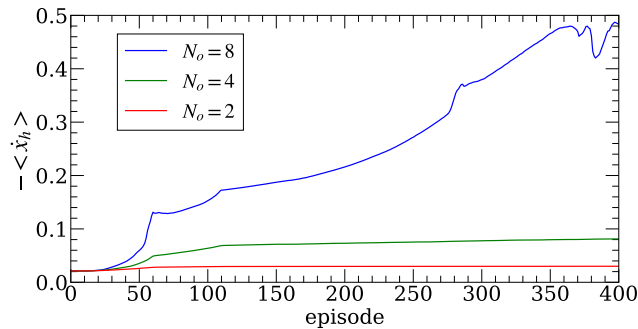


FIG. 7. Learning history of the swimming problem for different number of observables. $\langle \dot{x}_h \rangle$ is the time-averaged \dot{x}_h within an episode.

IV. CONCLUSION

Existing reinforcement learning algorithms for fluid control are inefficient under a small number of observables even if the flow is laminar. By incorporating the low-dimensional nature of the dissipative system into the learning algorithm, we resolved this problem and presented a framework for reinforcement learning that stably optimizes the policy for a small number of observables. In the practical application of a learning process in a fluid, a learning agent often cannot know any information about flow state except its own motion. For example, a swimming organism can learn how to swim underwater only from the time series of its swimming speed and its motion of moving parts as the example in the subsection III-C. In such a situation, the algorithm in this paper can efficiently find for the optimum control method. However, the present algorithm cannot handle a flow with large external noise; an inflow with white noise causes the attractor dimension infinite.

As demonstrated in previous studies, the orbit of flow hardly reaches the attractor during the learning process in the probabilistic policy framework. This leads to inefficient optimization around the attractor. Moreover, the deterministic policy described in this paper enables stable

optimization on an attractor, and it is not necessary to learn the processes repeatedly.

Although the proposed algorithm is simple, the value function can be approximated using a neural network as in deep reinforcement learning, instead of the generalized linear model of form (11). A more complicated regression model may be applied instead of the linear regression model of (15). In addition, although on-policy-type learning was used in this study, the proposed algorithm can be easily modified to the off-policy type to emphasize exploration.

ACKNOWLEDGMENTS

This work was supported by JSPS KAKENHI Grant Number JP17K14588. Simulations were performed on the “Plasma Simulator” (NEC SX-Aurora TSUBASA) of NIFS with support from the NIFS Collaboration Research program (NIFS19KNSS124).

DATA AVAILABILITY

The source codes that generate the results of this study are openly available in GitHub repository³⁶.

REFERENCES

- ¹S. L. Brunton, B. R. Noack, and P. Koumoutsakos, “Machine learning for fluid mechanics,” *Annual Review of Fluid Mechanics* **52**, 477–508 (2020).
- ².
- ³V. François-Lavet, P. Henderson, R. Islam, M. G. Bellemare, and J. Pineau, “An introduction to deep reinforcement learning,” arXiv preprint arXiv:1811.12560 (2018).
- ⁴D. Silver, T. Hubert, J. Schrittwieser, I. Antonoglou, M. Lai, A. Guez, M. Lanctot, L. Sifre, D. Kumaran, T. Graepel, *et al.*, “Mastering chess and shogi by self-play with a general reinforcement learning algorithm,” arXiv preprint arXiv:1712.01815 (2017).
- ⁵J. Janai, F. Güney, A. Behl, A. Geiger, *et al.*, “Computer vision for autonomous vehicles: Problems, datasets and state of the art,” *Foundations and Trends® in Computer Graphics and Vision* **12**, 1–308 (2020).

- ⁶S. Gu, E. Holly, T. Lillicrap, and S. Levine, “Deep reinforcement learning for robotic manipulation with asynchronous off-policy updates,” in *2017 IEEE international conference on robotics and automation (ICRA)* (IEEE, 2017) pp. 3389–3396.
- ⁷M. Gazzola, B. Hejazialhosseini, and P. Koumoutsakos, “Reinforcement learning and wavelet adapted vortex methods for simulations of self-propelled swimmers,” *SIAM Journal on Scientific Computing* **36**, B622–B639 (2014).
- ⁸M. Gazzola, A. A. Tchieu, D. Alexeev, A. de Brauer, and P. Koumoutsakos, “Learning to school in the presence of hydrodynamic interactions,” *Journal of Fluid Mechanics* **789**, 726–749 (2016).
- ⁹G. Novati, S. Verma, D. Alexeev, D. Rossinelli, W. M. Van Rees, and P. Koumoutsakos, “Synchronisation through learning for two self-propelled swimmers,” *Bioinspiration & biomimetics* **12**, 036001 (2017).
- ¹⁰F. Guéniat, L. Mathelin, and M. Y. Hussaini, “A statistical learning strategy for closed-loop control of fluid flows,” *Theoretical and Computational Fluid Dynamics* **30**, 497–510 (2016).
- ¹¹G. Reddy, A. Celani, T. J. Sejnowski, and M. Vergassola, “Learning to soar in turbulent environments,” *Proceedings of the National Academy of Sciences* **113**, E4877–E4884 (2016).
- ¹²G. Reddy, J. Wong-Ng, A. Celani, T. J. Sejnowski, and M. Vergassola, “Glider soaring via reinforcement learning in the field,” *Nature* **562**, 236–239 (2018).
- ¹³S. Verma, G. Novati, and P. Koumoutsakos, “Efficient collective swimming by harnessing vortices through deep reinforcement learning,” *Proceedings of the National Academy of Sciences* **115**, 5849–5854 (2018).
- ¹⁴Y. Zhu, F.-B. Tian, J. Young, J. C. Liao, and J. C. Lai, “A numerical study of fish adaption behaviors in complex environments with a deep reinforcement learning and immersed boundary–lattice boltzmann method,” *Scientific Reports* **11**, 1–20 (2021).
- ¹⁵H. Koizumi, S. Tsutsumi, and E. Shima, “Feedback control of karman vortex shedding from a cylinder using deep reinforcement learning,” in *2018 Flow Control Conference* (2018) p. 3691.
- ¹⁶J. Rabault and A. Kuhnle, “Accelerating deep reinforcement learning of active flow control strategies through a multi-environment approach,” arXiv preprint arXiv:1906.10382 (2019).
- ¹⁷H. Tang, J. Rabault, A. Kuhnle, Y. Wang, and T. Wang, “Robust active flow control over a range of reynolds numbers using an artificial neural network trained through deep reinforcement learning,” *Physics of Fluids* **32**, 053605 (2020).
- ¹⁸R. Paris, S. Beneddine, and J. Dandois, “Robust flow control and optimal sensor placement using deep reinforcement learning,” arXiv preprint arXiv:2006.11005 (2020).

- ¹⁹M. Tokarev, E. Palkin, and R. Mullyadzhyanov, “Deep reinforcement learning control of cylinder flow using rotary oscillations at low reynolds number,” *Energies* **13**, 5920 (2020).
- ²⁰D. Fan, L. Yang, M. S. Triantafyllou, and G. E. Karniadakis, “Reinforcement learning for active flow control in experiments,” arXiv preprint arXiv:2003.03419 (2020).
- ²¹G. Beintema, A. Corbetta, L. Biferale, and F. Toschi, “Controlling rayleigh–bénard convection via reinforcement learning,” *Journal of Turbulence* **21**, 585–605 (2020).
- ²²E. Hachem, H. Ghraieb, J. Viquerat, A. Larcher, and P. Meliga, “Deep reinforcement learning for the control of conjugate heat transfer,” *Journal of Computational Physics* , 110317 (2021).
- ²³J. Viquerat, J. Rabault, A. Kuhnle, H. Ghraieb, A. Larcher, and E. Hachem, “Direct shape optimization through deep reinforcement learning,” *Journal of Computational Physics* **428**, 110080 (2021).
- ²⁴S. Pawar and R. Maulik, “Distributed deep reinforcement learning for simulation control,” *Machine Learning: Science and Technology* **2**, 025029 (2021).
- ²⁵G. Novati, H. L. de Laroussilhe, and P. Koumoutsakos, “Automating turbulence modelling by multi-agent reinforcement learning,” *Nature Machine Intelligence* **3**, 87–96 (2021).
- ²⁶P. Garnier, J. Viquerat, J. Rabault, A. Larcher, A. Kuhnle, and E. Hachem, “A review on deep reinforcement learning for fluid mechanics,” arXiv preprint arXiv:1908.04127 (2019).
- ²⁷J. Rabault, F. Ren, W. Zhang, H. Tang, and H. Xu, “Deep reinforcement learning in fluid mechanics: A promising method for both active flow control and shape optimization,” *Journal of Hydrodynamics* **32**, 234–246 (2020).
- ²⁸R. Temam, *Infinite-dimensional dynamical systems in mechanics and physics*, Vol. 68 (Springer Science & Business Media, 2012).
- ²⁹D. Silver, G. Lever, N. Heess, T. Degris, D. Wierstra, and M. Riedmiller, “Deterministic policy gradient algorithms,” (2014).
- ³⁰R. S. Sutton, D. McAllester, S. Singh, and Y. Mansour, “Policy gradient methods for reinforcement learning with function approximation,” *Advances in neural information processing systems* **12**, 1057–1063 (1999).
- ³¹A. Rahimi and B. Recht, “Weighted sums of random kitchen sinks: Replacing minimization with randomization in learning,” in *Advances in neural information processing systems* (2009) pp. 1313–1320.
- ³²F. Pedregosa *et al.*, “Scikit-learn: Machine learning in python,” *the Journal of machine Learning research* **12**, 2825–2830 (2011).

- ³³J. Rabault, M. Kuchta, A. Jensen, U. Réglade, and N. Cerardi, “Artificial neural networks trained through deep reinforcement learning discover control strategies for active flow control,” *Journal of Fluid Mechanics* **865**, 281–302 (2019).
- ³⁴J. Schulman, F. Wolski, P. Dhariwal, A. Radford, and O. Klimov, “Proximal policy optimization algorithms,” arXiv preprint arXiv:1707.06347 (2017).
- ³⁵M. Uhlmann, “An immersed boundary method with direct forcing for the simulation of particulate flows,” *Journal of Computational Physics* **209**, 448–476 (2005).
- ³⁶K. Akira and S. Masaki, “<https://github.com/rl-for-fluid>,” (2021).